Near-Field Microlensing and Its Effects on Stellar Transit Observations by *Kepler*

Kailash C. Sahu & Ronald L. Gilliland

Space Telescope Science Institute, Baltimore, MD 21218

ksahu@stsci.edu, gillil@stsci.edu

ABSTRACT

In this paper, we explore the astrophysical implications of near-field microlensing and its effects on stellar transit observations, with a special emphasis on the *Kepler* mission. *Kepler* is a NASA-approved mission whose goal is to detect a large number of extrasolar, earth-like planets by obtaining near-continuous photometry of $> 100,000$ F, G, and K dwarfs for four years. The expected photometric precision of *Kepler* is 90 μmag (achieved in 15 minute samples), at which the effect of microlensing by a transiting companion can be significant. For example, for a solar-type primary transited by a white-dwarf secondary, the maximum depth of the transit is 0.01%, which is almost entirely compensated by the microlensing amplification when the white dwarf is at $\sim$0.05 AU. The combined effect of microlensing and transit increases to a net amplification of 150 μmag at an orbital separation of 0.1 AU, and 2.4 millimag at an orbital separation of 1 AU. Thus, the effect of microlensing can be used to break the degeneracy between a planetary-mass object for which the microlensing effect is negligible, and a more massive object of the same size. For brown dwarfs at orbital separations of a few AU, the effect of microlensing is several percent of the transit depth, and hence the microlensing effect must be taken into account in deriving the physical parameters of the brown dwarf. The microlensing signal caused by a neutron star or a black hole in a binary can be several millimag, far exceeding the transit depth, and potentially detectable even from ground-based observations. *Kepler* will be sensitive to white dwarfs, neutron stars, and black holes in binaries through their microlensing signatures. These observations can be used to derive the frequency of such compact objects in binaries, and to determine their masses.

1. Introduction

In a transit experiment where the goal is to look for obscuration of light caused by the transiting body, the effect of microlensing by the transiting body is generally thought to be negligible. The main reason is the following: for orbital separations of a few AU, the Einstein ring due to a stellar companion (the lens) is typically much smaller than the size of the primary (the source), so that the maximum amplification caused by the lens is small. In addition, the lens has a finite size, which may cause one or more of the rays to be occulted, which makes the effect of microlensing small compared to the obscuration caused by the lens. In principle however, the effect of microlensing can be important, and this effect becomes more important when the binary companion is a degenerate star (i.e. massive but small) or if the orbital separation is large. Gould (1995) argued that self-lensing in binaries in which at least one member is an ordinary (non-compact) star (assuming $\gtrsim 0.3$ mag amplification) would be exceedingly rare. Marsh (2001) argued for better prospects in finding microlensing signatures in main-sequence, white dwarf binaries, but also concluded that finding microlensing in binaries containing neutron stars or black holes is unlikely. At high photometric precision, however, microlensing effects at *much* lower amplitude can be important, and this effect must be taken into account in interpreting the observed light curves.

The Discovery-class mission, *Kepler: A Search for Terrestrial Planets*, with an expected launch in 2007, is a high-precision photometric mission whose main goal is to detect a statistically large number of extrasolar, earth-like planets, if such planets are common around stars in the extended solar-neighborhood. *Kepler* will provide such detections by obtaining extensive (four years), near-continuous photometry on the same set of over 100,000 stars at typical transit-depth precisions of 90 parts per million on the 15 minute sampling rate for $V \sim 12$ stars. An Earth-analogue transit will typically last $\sim$10 hours and be detected at $\sim$6 σ per event which repeats once per year. (More details on *Kepler*, which is a NASA-approved discovery-class mission, can be found at http://www.kepler.arc.nasa.gov/). At such precision, the effect of microlensing by a transiting compact and massive body can often be significant. For example, when the lens is a compact object such as a white dwarf or a neutron star, the effect of microlensing can far exceed the transit signal, causing a net positive amplification. The microlensing contribution due to a brown dwarf at 1 AU would be several percent of the transit depth. In this paper, we explore the astrophysical implications of such microlensing in the near-field limit of a lens orbiting the source, with particular emphasis on the upcoming *Kepler* mission.

2. Microlensing vs. Transit

Gravitational microlensing studies over the past decade have revealed large numbers of events toward the Magellanic Clouds and the Galactic Bulge (Alcock et al. 2000; Udalski 2000; Lassere et al. 2001). With near real-time analysis of the photometry, many of the microlensing events are detected early enough to provide alerts allowing for close and intense follow-up monitoring of potentially interesting events. Such intense monitoring has been carried out for several purposes such as, to look for planets associated with the lens (Albrow et al. 2001a; Gaudi et al. 2002); to determine limb-darkening parameters of the source (Albrow et al. 2001b); to measure lens masses through parallax effects and orbital motions of binary lenses (An et al. 2002); to determine the caustic crossing time-scales to determine the lens location (Afonso et al. 2000), etc. The literature on microlensing both from observational and theoretical perspectives is now quite large and mature (e.g. Schneider et al. 1993, Paczyński, 1996 & Gould, 2001).

By contrast, the much simpler effect of geometric obscuration resulting in transits as one object passes in between a source and the observer has received much less attention relative to microlensing (unless one includes binary star eclipses in this context), although there has been a surge of interest on this topic recently. In the case of classical microlensing the events are rare, thus the successful projects monitor very dense stellar fields with large format detectors. However, the microlensing signal can be quite large, so these projects require only modest precision. Transits of planets generally provide much smaller signals: Jupiter transiting the Sun, for example, would yield an event of 1% depth. Furthermore, the inclinations are expected to be random, so for planets with orbital radii of $\gtrsim$1 AU, >99% of the existing systems would not exhibit transits due to the small chance of having the required alignment. For terrestrial planets the transit depth is even smaller: about one part in 10,000. Hence, although seeking evidence of Earth-like, extrasolar planets (i.e., having a size comparable to the Earth at a distance of about an AU from a solar-analogue host star) via transits has long been advocated as a means to search for terrestrial planets (Borucki and Summers 1984), this is a challenging experiment. With the stable observing conditions provided by observations from space and the ability to mosaic a significant number of CCDs it has become feasible to detect true Earth-like extrasolar planets with a modest, dedicated mission such as *Kepler*.

In a mission with such unprecedented photometric accuracy, it is obviously important to make sure that the signature of an earth-like planet is unique. Since a white dwarf has a radius comparable to that of the Earth, a white dwarf in a one year orbit transiting a solar-like star could in principle mimic the signature of a terrestrial planet (although this can be easily eliminated in most cases by follow up radial velocity measurements). This study is motivated by asking if the photometric signal itself due to microlensing by the white dwarf, even though it is only 1 AU from its host star, might be detectable. Indeed for the case of a white dwarf in a one year orbit, the geometric obscuration effect is at the level of one part in 10^4, but the microlensing effect is much larger, amounting to a few parts in 10^3. As we will show later, the light curve caused by the microlensing has a form very similar to the transit light curve with a change of sign. Taking into account the effect of gravitational microlensing, we will show that white dwarfs transiting main sequence stars with orbital periods of $\gtrsim$3 days would produce *positive* intensity signals, and hence will not be a source of confusion with terrestrial planets for *Kepler*. The purpose of this paper is to establish the framework for calculating microlensing in this near-field regime, to establish domains in source and lens characteristics where the effect is measurable, and to explore whether the near-field microlensing signal can be exploited to return astrophysical information such as the lens mass. In §3 we discuss the amplification in the near-field regime and present a generalized formalism for generating light curves taking the finite source size, the finite lens size, the inclination of the orbit and the limb-darkening parameters into account, and discuss how the simpler cases of point source etc. can be considered as special cases of this generalized case. In §4, we discuss the amplifications caused by various types of degenerate and non-degenerate secondaries at different orbital separations for different types of sources, and discuss the interesting cases in which the gravitational light amplification and geometric obscuration effects are similar in amplitude. §5 is devoted to a more detailed discussion of special cases such as Earth-mass planets, Jupiters, brown dwarfs, white dwarfs, neutron stars and black holes as secondaries in orbit around main sequence stars. We conclude in §6 with a summary of earlier sections and further discussion on the prospects of such observations with the upcoming *Kepler* mission, and the possible astrophysical returns from such observations.

3. Microlensing with Finite Source and Finite Lens

Some early theoretical work involving a finite source (and a point lens) was carried out by Bontz (1979). A mathematical description leading to an analytical solution for such a case can be found in Schneider et al. (1992) and Witt and Mao (1994). Dominik (1998) and Gould & Gaucherel (1997) have independently developed efficient schemes for calculating the finite source effects using Green's theorem and line integrals instead of following the conventional approach of 2-dimensional integration over the source. The numerical recipe developed by Sahu (1994 a,b) uses a polar coordinate system centered on the source, which is particularly useful in considering radially-symmetric effects such as the limb darkening, which is followed here.

The effect due to a finite *lens* has received much less attention; nevertheless this has been discussed in some detail by Bromley (1996) and Marsh (2001), and more recently by Agol (2002) and Beskin and Tuntsov (2002). The literature dealing with the combined effect of both a finite source and a finite lens is generally lacking. Gould (1995) considered the effect of microlensing in binaries and concluded that only pairs of pulsars would be interesting. However, his analysis was done in the frame-work of the "standard" microlensing where the source lies within the Einstein ring radius of the lens, in which case the amplification may be more than 34%. Marsh (2001) has generated light curves for compact, degenerate binaries with small orbital separations, where he assumed that the source is uniformly bright and that the fainter of the two images is occulted by the lens. In order to ensure that the results are valid for all cases observed by *Kepler*, our calculations take appropriate limb-darkening parameters into account, and do not assume *a priori* that the fainter image is occulted.

In the following section, we discuss in detail the approach adopted here in determining the effect of finite sizes of the source and the lens simultaneously. Our light curve simulations are valid for low-mass as well as high-mass binaries at any orbital separation, and also include an appropriate limb-darkening for the source and different inclinations of the orbital plane. We note that in the extreme case where the lens is a point lens, the net effect would be the same as that of pure microlensing. In the extreme case where the lens mass is zero, the effect would be the same as that of a pure transit.

3.1. Formalism for Light Curve Simulation

Let us first consider the source to be a point source. Let D_L be the distance to the lens (L), D_{LS} be the distance from the lens to the source (S), and D_S be the distance from the observer to the source as shown in Fig. 1. Let R_s represent the distance between the center of the lens and the source projected onto the lens plane.

The radius of the Einstein ring at the lens plane, R_E, can be written as

$$R_E^2 = \frac{4GM_L D}{c^2}, \qquad D \equiv \frac{D_{LS} D_L}{D_S} \tag{1}$$

where M_L is the the mass of the lens.

The lens produces two images of the source, S' and S'', as shown in Fig. 1. At the lens plane, these two images are situated on the line joining the source and the center of the lens, one inside and the other outside the Einstein ring. The distance between the lens and the two images can be expressed as (e.g. see Paczyński 1996 for details)

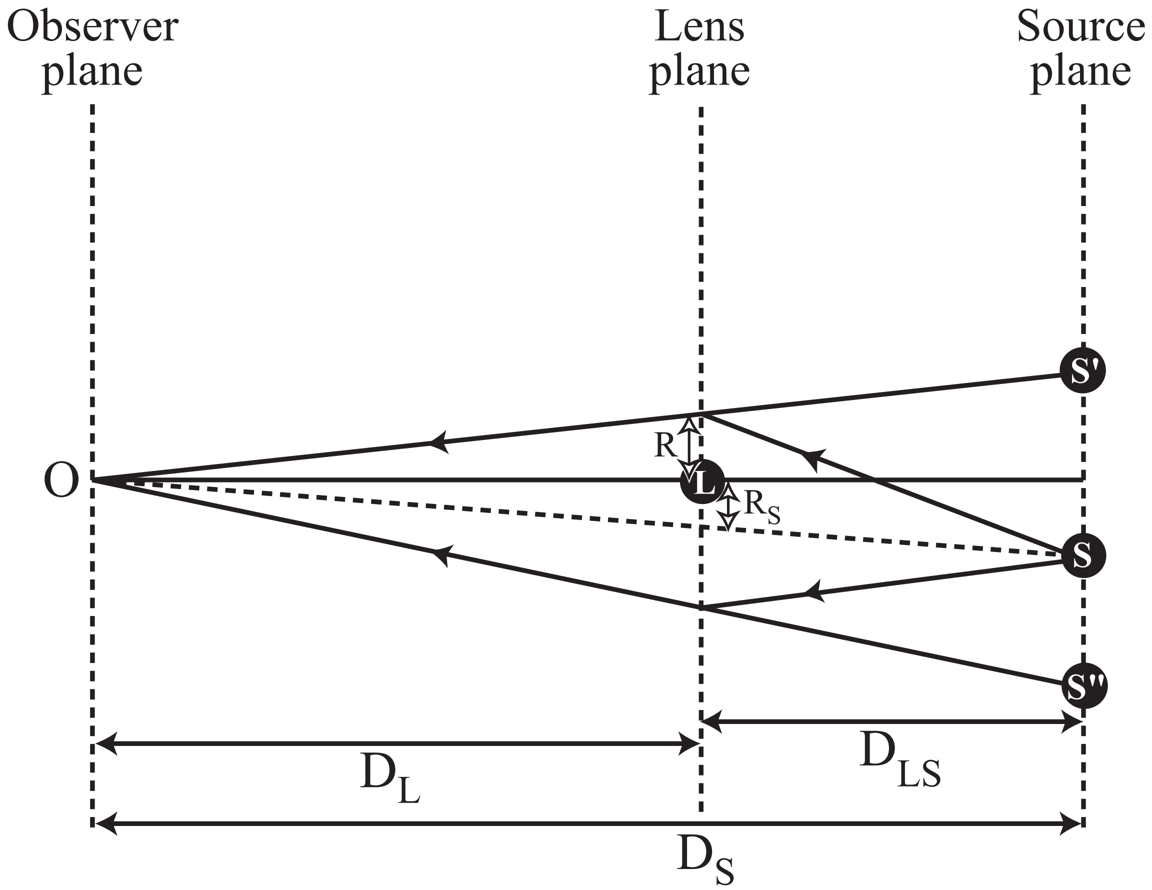

Fig. 1.— The geometry of the gravitational lensing is schematically shown here. The observer, the lens and the source are located at positions O, L and S, respectively. D_L is the distance to the lens, D_S is the distance to the source, and D_{LS} is the distance from the lens to the source. The lens (L) produces two images of the source at positions S' and S''. At the lens plane, the lens, source and the two images lie on a straight line. S' corresponds to the brighter image which is formed outside the Einstein ring and is at least as bright as the source itself. S'' corresponds to the fainter image which is formed inside the Einstein ring.

$$R_{+,-} = 0.5[R_s \pm (R_s^2 + 4R_E^2)^{1/2}] \tag{2}$$

.

The amplification of these two images are given by

$$A_p^{+,-} = \frac{u^2+2}{2u(u^2+4)^{1/2}} \pm 0.5, \qquad u \equiv R_s/R_E \tag{3}$$

.

Thus we see that the image outside the Einstein ring is the brighter of the two images, and is at least as bright as the source itself. The combined amplification A_p for a point source is given by

$$A_p = A_p^+ + A_p^- = \frac{u^2+2}{u(u^2+4)^{1/2}} \tag{4}$$

If u is replaced by the minimum impact parameter u_0, we get the maximum amplification A_p^0.

Let us now discuss the case of an extended source, which can be treated as an ensemble of point sources. We will assume the lens to be extended, opaque and spherically symmetric. For an extended source, it is convenient to work in the lens plane, and Fig. 2 schematically shows such a case, where the source is larger than the Einstein ring itself. The two circles A and B represent two parts of the source, whose images are (A′, A″) and (B′, B″), respectively. The brighter images (A′ and B′) are outside the Einstein ring, none of which (A′) is occulted by the lens. The fainter images (A″, B″) are inside the Einstein ring, one of which (A″) is occulted by the lens. It is worth noting that the images of all the parts of the source are displaced with respect to the original positions such that no two images overlap. Microlensing preserves the surface brightness, and any amplification caused by microlensing is caused by a proportional increase in the size of the image with respect to the original size.

The amplification of an extended source would then be given by (equation 6.81 of Schneider et al. 1993)

$$A = \frac{\int d^2y \; I(y) \; A_p(y)}{\int d^2y \; I(y)} \tag{5}$$

where $I(y)$ is the surface brightness profile of the source, $A_p(y)$ is the amplification of a point source at position y, and the integration is carried out over the entire surface of the source.

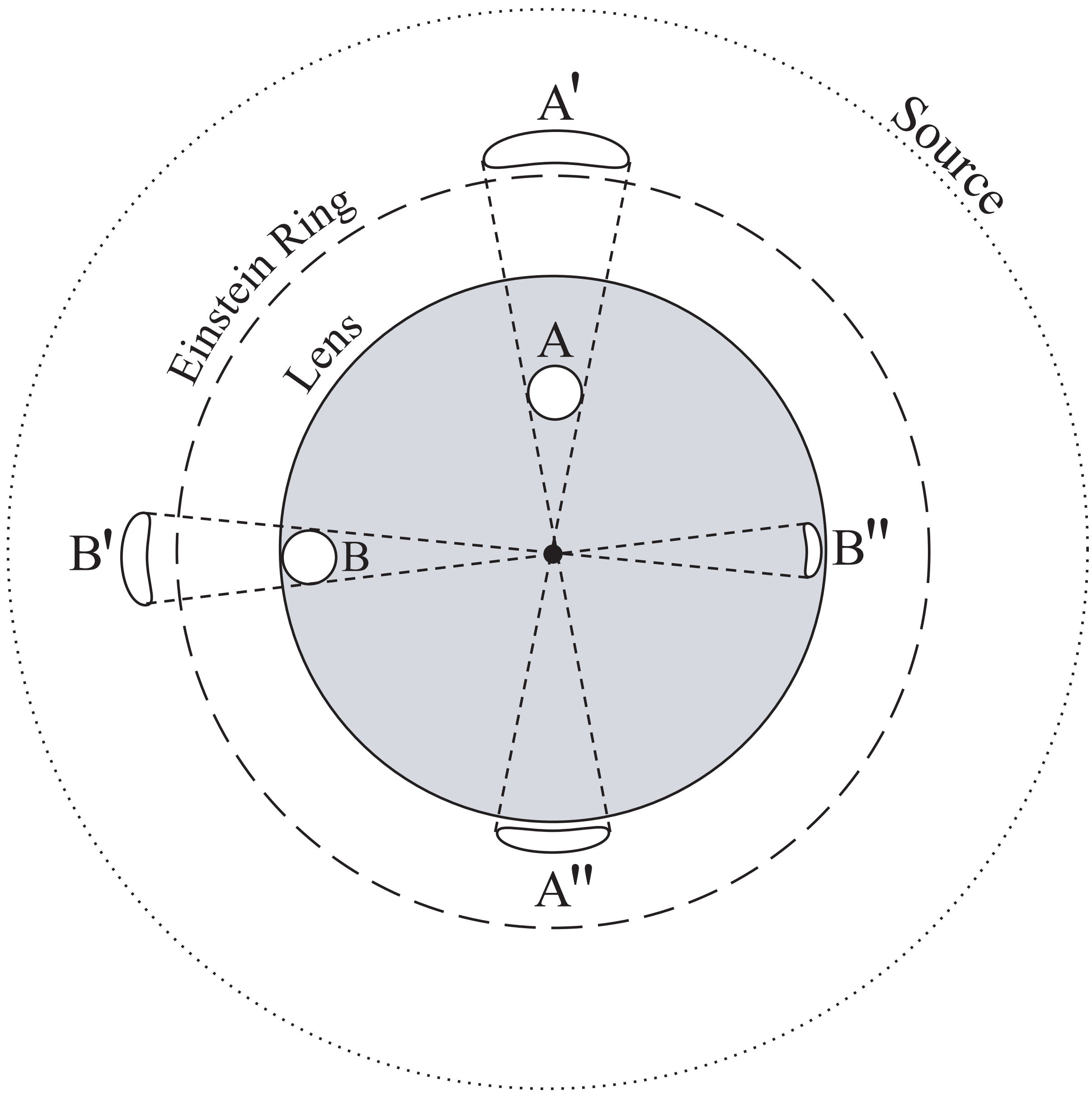

Fig. 2.— A schematic showing the positions of the lens, the source and the images in the lens plane. The solid circle is the lens, the dashed circle is the Einstein ring, and the dotted circle is the source. The circle A represents a part of the source whose images are A′ and A''. None of these two images are occulted by the lens. The circle B represents a part of the source farther away from the lens, whose images are B′ and B''. Notice that the fainter image corresponding to B″ is occulted by the lens, whereas the brighter image corresponding to B′ is not occulted.

For a lens with finite size, the above equation must be rewritten as

$$A = \frac{\int d^2y \; I(y) \; [A_p^+(y) + A_p^-(y)]}{\int d^2y \; I(y)} \tag{6}$$

where the integration is carried out over all the points in the image plane which are not occulted by the lens.

Note that for a finite-size, uniformly bright source, the maximum amplification (corresponding to a point lens which is perfectly aligned with the source) is given by

$$A_{max} = [1 + \frac{4R_E^2}{r_S^2}]^{\frac{1}{2}} \tag{7}$$

where r_S is the radius of the source scaled to the lens plane.

In order to carry out the integration given by equation (6), let us follow Fig. 3 where R_s is the distance between the lens and the center of the source projected onto the lens plane, and l is the impact parameter (the minimum distance between the center of the lens and the center of the source at the lens plane as the lens traces the path shown in the figure). Let us choose a circular coordinate system and let (r, θ) be the representative point which is at a distance y from the lens. From Fig. 3 we see that

$$y = \sqrt{R_s^2 + r^2 - 2 \; R_s \; r \; cos(\gamma)} \tag{8}$$

where

$$R_s = \sqrt{x_0^2 + l^2}, \;\; \gamma = \pi - \theta - \alpha \; and \; \alpha = sin^{-1}(l/R_s) \tag{9}$$

i.e.

$$y = \sqrt{R_s^2 + r^2 + 2 \; R_s \; r \; cos(\alpha + \theta)} \tag{10}$$

The two images of the point (r, θ) are formed at distances y_+ and y_- from the center of the lens along the line joining the lens and the point (r, θ) such that

$$y_{+,-} = 0.5[y \pm (y^2 + 4R_E^2)^{1/2}] \tag{11}$$

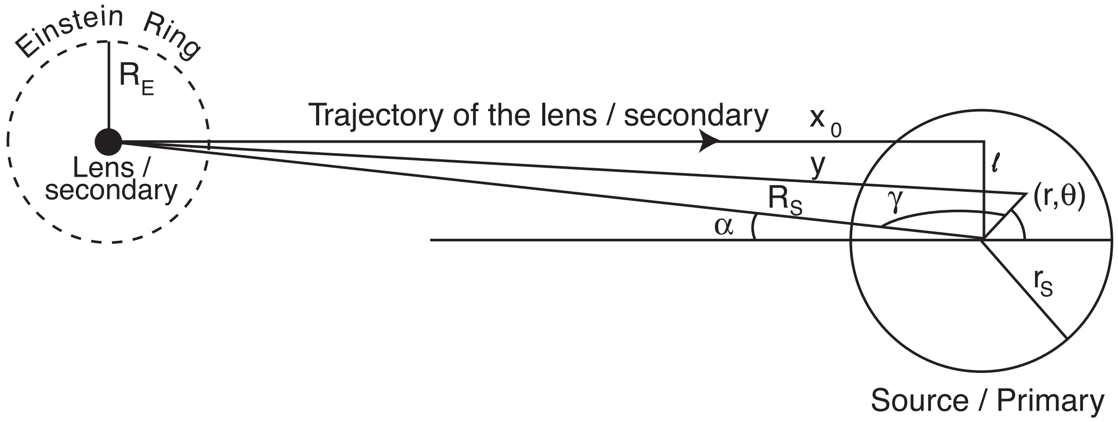

Fig. 3.— The geometry used for calculating the microlensing and the transit contributions, taking the effect of the extended source and the extended lens into account. l is the minimum impact parameter and r_S is the source radius. A polar coordinate system is defined as shown here to integrate over the source. The effect of the inclination (not shown in the figure) is taken into account through appropriate changes in the impact parameter. We take the effect of the transit and the microlensing simultaneously into account by taking the deflections and amplifications of the unocculted rays from every point in the source. To check the correctness of the algorithm used, the contribution of a pure transit was calculated in two ways: by specifying the mass of the lens to be zero, and by forcing the deflections caused by the gravitational potential of the lens to be zero. Both gave identical results as expected.

.

The image is not occulted if

$$y_{+,-} > r_l \tag{12}$$

where r_l is the radius of the lens.

The amplification corresponding to these two images can be written as

$$A_{+,-}(y) = \frac{(y/R_E)^2 + 2}{2(y/R_E)[(y/R_E)^2 + 4]^{1/2}} \pm 0.5 \tag{13}$$

In calculating the combined amplification $A(y) = A_+(y) + A_-(y)$, we consider only the images which satisfy the condition (12) to ensure that the image is not occulted by the lens.

Using equation(6), the total amplification can be calculated by integrating over the source using

$$A = \frac{\int_0^{r_S} \int_0^{2\pi} A(y)\ I(y)\ dr\ d\theta}{\int_0^{r_S} \int_0^{2\pi} I(y)\ dr\ d\theta} \tag{14}$$

This is an expression suitable for numerical integration which will take the finite size of both the lens and the source into account. The light curve can be reproduced as a function of time t, which is related to x_0 through the relation $x_0 = (R_E/t_0)t$ where t_0 is the timescale of microlensing (which is the time taken by the lens to cross its own Einstein ring). y in turn, is related to x_0 through equation 8 and 9.

Since we are mostly interested in the effect caused by the secondary in a binary, we need to include the effect of the inclination, which can be incorporated through a suitable choice of the minimum impact parameter. The light curves can then be calculated with the amplification as a function of the phase (see Fig. 3).

3.2. Determination of the Lens Mass

We also provide here the equations that allow the mass of the lens to be derived from photometry in the limit where microlensing amplification dominates the light curve, as for example would be the case for a white dwarf orbiting a main-sequence star at 1 AU. If multiple, periodically repeating events have been observed, Kepler's law provides a relation between the orbital period (P), semi-major axis (a) and the sum of the masses:

$$P^2 = \frac{4\pi^2 a^3}{(M_S + M_L)G} \tag{15}$$

where M_S is the mass of the source which may be constrained from independent observations (such as spectroscopy and spectral classification and/or with radial velocity observations), and M_L is the lens mass for which an estimate is desired.

Assuming $D_{LS} \sim a << D_L$, equation (7) can be rewritten as

$$M_L = \frac{(A_0^2 - 1) r_S^2 c^2}{16 G a} \tag{16}$$

where r_S is the radius of the source star scaled to the lens plane, and c is the velocity of light. A_0 is the maximum amplification during the microlensing event which we have assumed to be $\sim A_{max}$. Note that for source sizes much larger than the Einstein ring radius, the maximum amplification during the microlensing event (A_0) is nearly equal to A_{max} given by equation 7 regardless of the impact parameter, provided that the lens actually transits the source. This is demonstrated by the flat-topped nature of the numerically-simulated lightcurves (Fig. 10, 14 and 15), and is consistent with discussions in several other papers (e.g. Agol 2002). Thus $A_0 \sim A_{max}$ is generally a good approximation. If independent observations provide constraints on the source radius, then equation (16) can be used to solve for orbital separation, a, and M_L.

An additional constraint comes from the duration of the transit (T_t) which, for a circular orbit and 90° inclination, can be written as

$$T_t = \frac{2 r_s P}{2\pi a} = \frac{2 a^{1/2} r_S}{[(M_L + M_S)G]^{1/2}} \tag{17}$$

.

Combining equations (16) and (17) to eliminate r_S

$$(A_0^2 - 1) T_t^2 = \frac{64 M_L a^2}{(M_L + M_S) c^2} \tag{18}$$

After a little algebra, this can be rewritten as

$$M_L = \frac{M_S (A_0^2 - 1) T_t^2 c^2}{64 a^2 - (A_0^2 - 1) T_t^2 c^2} \tag{19}$$

This equation can be used to derive the mass of the lens if M_S and a are known.

We can also combine equations (16) and (17) to eliminate a, and write

$$A_0^2 - 1 = \frac{4G^2 M_L(M_L + M_S)T_t^2}{c^2 r_S^4} \tag{20}$$

This equation can be solved to express the lens mass

$$M_L = \frac{[G^2 M_S^2 T_t^2 + (A_0^2 - 1)c^2 r_S^4]^{1/2} - GM_S T_t}{2GT_t} \tag{21}$$

This equation can be used to derive the mass of the lens if M_S and r_S are known.

We will return to a discussion of lens mass determination with an example in § 5.2.

3.3. Generalization to a limb-darkened source

Since the polar coordinate system we have chosen is centered on the source (Fig. 3, equation 8), it is easy to incorporate limb-darkening for the source which has an azimuthal symmetry. Recently, the limb darkening parameters were derived for HD 209458 using the high signal-to-noise observations obtained with the Space Telescope Imaging Spectrograph aboard Hubble Space telescope in the wavelength region 582 to 638 nm (Brown et al. 2001). Based on these observations, a limb-darkening of the form

$$I(\mu) = 1.0 - u_1(1-\mu) - u_2(1-\mu)^2 \tag{22}$$

was used, where μ is the cosine of the angle between the line of sight and the normal to the local stellar surface (Claret & Gimenez 1990). We have used $u_1 = 0.3$ and $u_2 = 0.35$ as applicable to HD 209458 in the wavelength region 582 to 638 nm, in generating all the light curves here. We should note, however, that the formalism discussed in this paper can be used to take any other specific form of the limb-darkening as well.

3.4. Special case: point lens and zero-mass lens

In the limiting case of a point lens, the results should be identical to the results obtained from other standard treatments of microlensing involving a finite source and a point lens. In particular, equation (7) can be directly used to calculate the amplification for the special case where the lens and the source are perfectly aligned. This provides a direct test (although only for the special case of a point lens) which was used to check the algorithm discussed above. The previous results obtained by Sahu (1994b) and confirmed by Dominik & Hirshfeld (1996) also served as a test case for a point lens, to check the correctness of the simulated light curves. We have also checked our calculations with a few special cases calculated by Marsh (2001) and obtained consistent results.

In the limiting hypothetical case where the mass of the lens is zero (but the size is finite), the results obtained here should be identical to the results obtained for pure transit. The transit light curve simulated by Brown et al (2001) for HD 209458 serves as a test case for this purpose. Our algorithm was used to simulate a light curve for HD 209458 using the same limb-darkening parameters suggested by Brown et al (2001). The resultant light curve was found to be identical to the one published by Brown et al (2001) which provided a further check on the validity of the algorithm used here.

The treatment for a zero-mass lens is equivalent to assuming that the images are not deflected, the amplification corresponding to the brighter image is one, and the amplification corresponding to the fainter image is zero. This, in turn, is equivalent to a restricted version of the algorithm where all deflections and amplifications are ignored. The light curves were simulated using both these approaches, and the resultant light curves were identical as expected.

4. Net amplifications for various secondaries

The maximum net amplification caused by a secondary companion (after taking the finite sizes for the source and the lens into account) generally corresponds to the configuration where the lens and the source are perfectly aligned (except in a few special cases where the maximum amplification occurs just before or after the egress as explained later). This configuration corresponds to $R_s = 0$ (equation 8), which can be used in equations (8-14) to calculate the amplification. An analytical solution for such a configuration was derived by Marsh (2001).

The maximum amplification thus calculated for a variety of secondaries (Jupiter, brown dwarf, white dwarf, neutron star and black hole) at various orbital separations are shown in figures 2 to 7, assuming $D_L >> D_{LS}$. Figs. 4-8 assume the source to be a solar type star with radius 7 $\times 10^{10}$cm. The radii and the masses assumed for the different secondaries are given in Table 1.

In most cases that we consider, the secondary (lens) will provide an amount of light in the system that is small compared to that from the primary (source). We therefore do not provide explicit corrections to light curves from the luminosity of the lens itself. We also note the obvious, yet subtle, point that the light from the lens is constantly present before, during and after an occultation/microlensing event. Therefore, during the transit the only effect from the light from the secondary is a dilution of the light curve changes in the same proportion as the secondary contributes to the total light light away from the transit. For a canonical case of a white dwarf orbiting a solar-like star in which the surface brightness of the two components are similar, the white dwarf will have a flux about 10^{-4} that of the primary implying a 0.01% dilution effect. (*Kepler* might be able to detect the secondary eclipse, and this would be interesting, but correcting for the minor change of inferred microlensing amplitude is not relevant). Exceptions to this rule can arise, e.g. when the primary is intrinsically small such as a brown dwarf, the amplifications of which are shown in Fig. 9. In the case of a white dwarf lensing a brown dwarf, this dilution effect could be a dominant effect which can be applied in a trivial manner using the expected luminosities of the two objects in the observational bandpass.

Fig. 4 shows the effects of different secondaries for orbital separations of 0 to 1 AU and Fig. 5 shows the same for orbital separations of 0 to 5 AU. Note that the radii of a Jupiter and a brown dwarf are identical. However, while the microlensing contribution due to a Jupiter is negligible, the microlensing contribution due to a brown dwarf is appreciable at Kepler's sensitivity even at 1 AU. As a result, the Δmag caused by these two types of secondaries are different at Kepler's sensitivity at 1 AU, which is shown in Fig. 4. This effect must be taken into account in deriving the radius of a brown dwarf (more details on such a case are given later).

For white dwarfs, neutron stars and black holes, the net effect is dominated by the microlensing at any orbital separation, and the transit contribution is negligible (Figs. 4-5).

Table 1: Secondary (Lens) Characteristics

Secondary	Radius ($R_\odot$)	Mass ($M_\odot$)
Jupiter	0.1	0.001
Brown Dwarf	0.1	0.05
White Dwarf	0.01	0.6
Neutron Star	2.8×10^{-5}	1.4
Black Hole	$< 1 \times 10^{-5}$	8.0

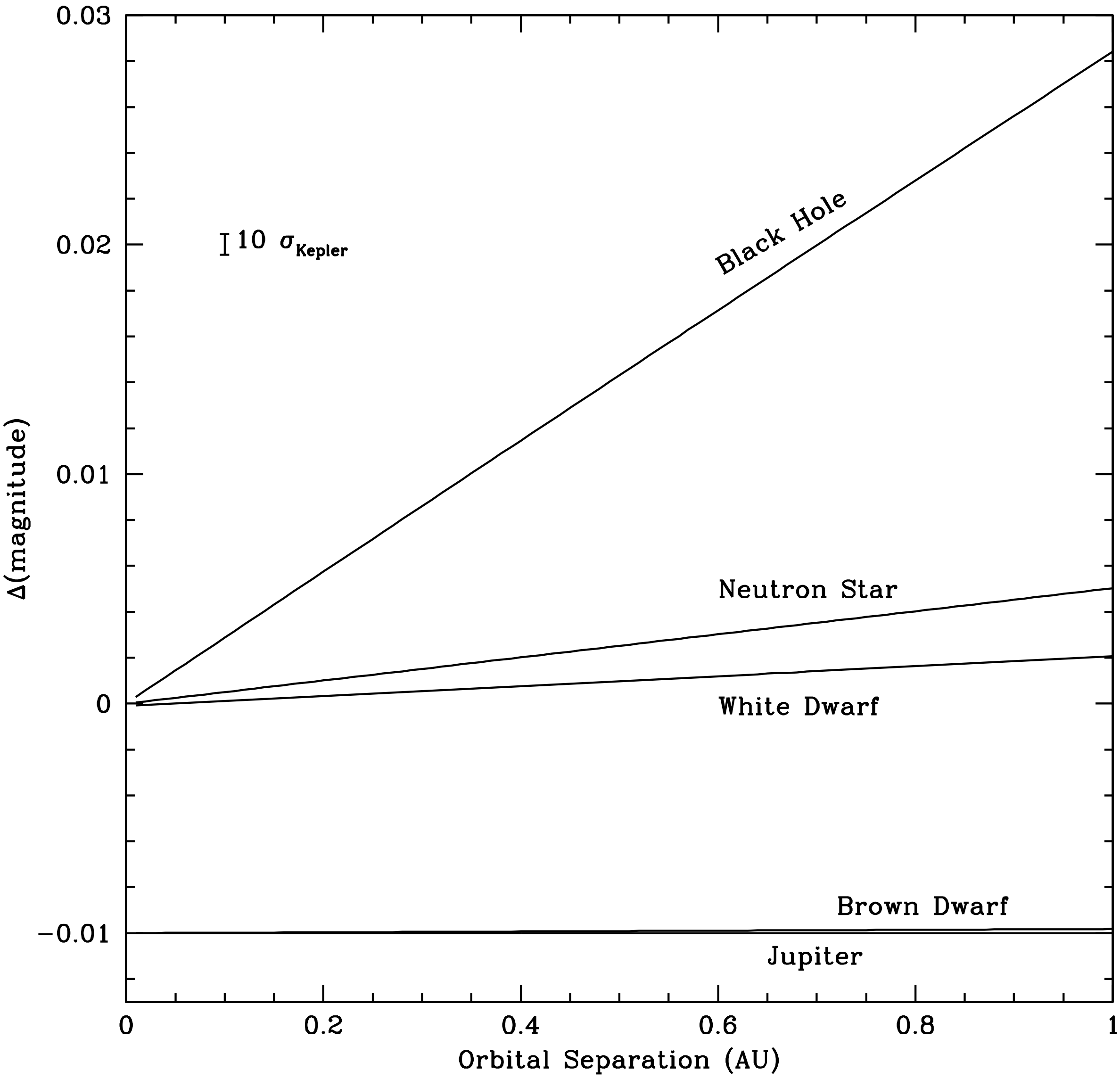

Fig. 4.— The net amplification caused by different types of secondaries is plotted as a function of orbital separation after taking both the transit and the microlensing contributions into account. See Table 1 for the details on the radii and the masses used for the different types companions. The source is assumed to be a solar type star, and the inclination is assumed to be 90°. The errors expected from the *Kepler* mission are too small to be shown in this scale, so the error bar shows 10 times σ_{Kepler} where σ_{Kepler} refers to the expected photometric error per 15-minute sample at $V = 12$. Note that at 1 AU, the amplification caused by a black hole secondary is ~2.5% which is within reach of ground-based observations, and could be detectable in ground-based survey programs such as OGLE III.

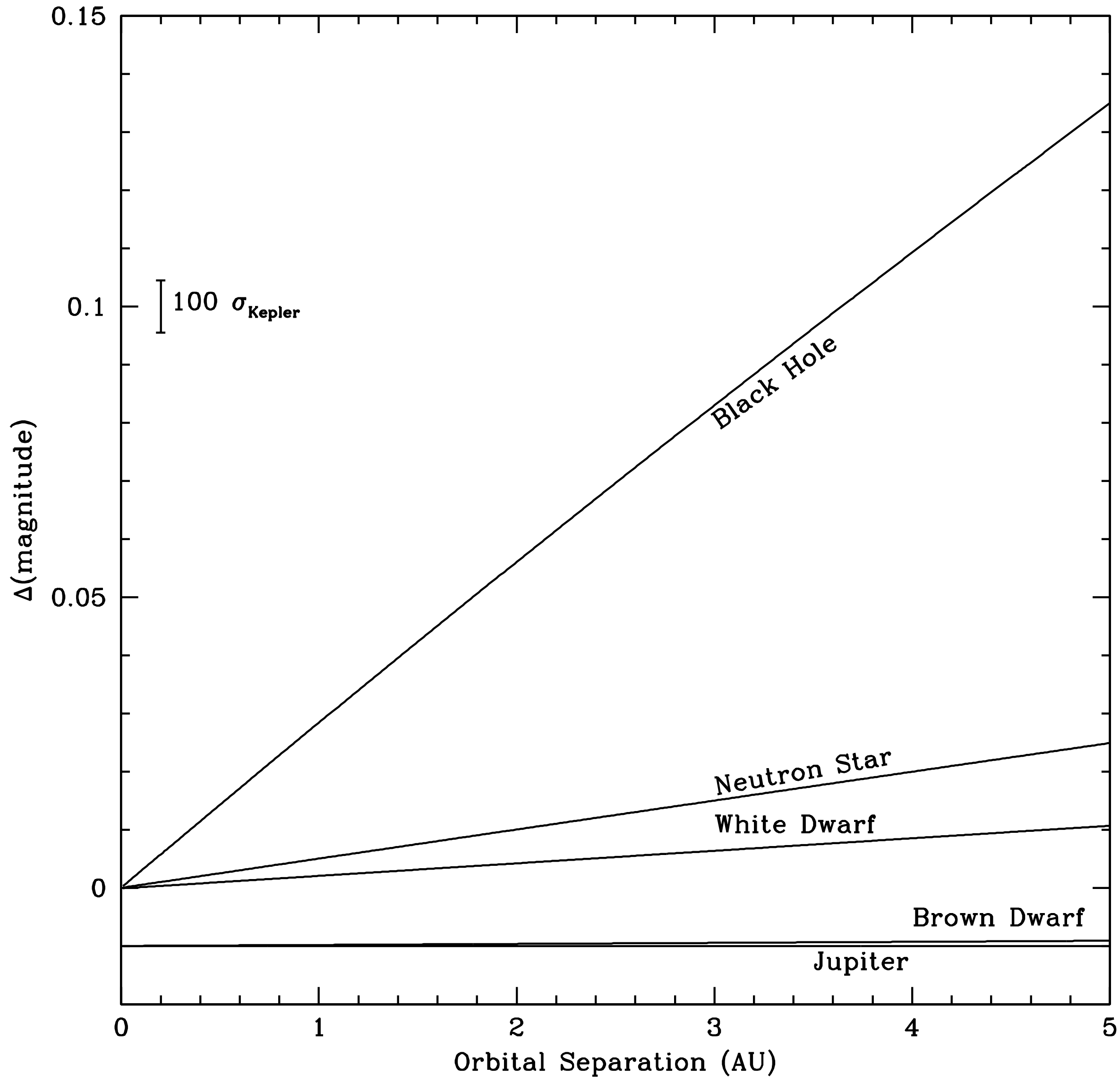

Fig. 5.— Same as the previous figure but for a larger range of orbital separations (0 to 5 AU). The error bar shown here corresponds to 100 times σ_{Kepler}. At an orbital separation of 5 AU, the amplification caused be a white dwarf is more than 10 millimagnitudes. The amplifications caused by neutron star and black hole binaries at 5 AU would be well within the reach of ground-based survey programs.

In order to show the *Kepler* sensitivity, it had to be multiplied by factors of 10 and 100 in Figs. 4 and 5, respectively. The net effects caused by the neutron star and the black hole at 1 AU, 5 and 30 millimag respectively, are large enough in principle to be detectable even from ground-based observations.

An enlarged view of the effects of the brown dwarf and Jupiter are shown in Fig. 6 and Fig. 7, for orbital separations of 0-5 AU and 0-100 AU, respectively. As seen from Fig. 6, the microlensing contribution due to a brown dwarf is significant even for small orbital separations and must be taken into account in estimating its radius from the observed light curves. Even for a Jupiter-mass secondary, the microlensing contribution starts to become relevant at orbital separations of 5 AU or more at *Kepler*'s sensitivity. From Fig. 7 we see that the microlensing contribution from a brown dwarf almost exactly cancels out the transit contribution at an orbital separation of ∼55 AU, beyond which the net amplification is positive.

An enlarged view of the effects of the white dwarf, neutron star and black hole are shown in Fig. 8 for small orbital separations of 0 to 0.1 AU. For neutron star and black hole secondaries, the net amplification is positive at any orbital separation. For a white dwarf, the microlensing contribution almost exactly cancels out the transit contribution at ∼0.05 AU, beyond which the net amplification is positive.

The effect of microlensing is more dramatic if the size of the source is smaller, as is the case for a brown dwarf. Fig. 9 shows such a case where we assume the size of the source to be 7×10^9 cm, as applicable for a brown dwarf or a Jupiter. The amplification, which is the ratio of the amplified luminosity and the original luminosity, is typically much larger compared to the earlier case of a solar type source.

The expected amplification is a function of inclination, which is shown in Fig. 10. The solid curve is the expected maximum transit depth, and the dotted curve shows the expected amplification at mid point taking both the transit and the microlensing into account. Here the source (primary) is assumed to be a solar type star and lens (secondary) is a white dwarf at an orbital separation of 1 AU.

To show the relative importance of microlensing and transit for various kinds of secondaries at different orbital separations, we have plotted in Fig. 11 the orbital radius at which the microlensing signal equals the transit signal as a function of the mass of the secondary. For example, for a white dwarf secondary, the expected transit depth, given by r_L^2/r_S^2, where r_L and r_S are the radii of the secondary (lens) and the primary (source) respectively, is 0.0001 and the mass of the lens is 0.6 $M_\odot$. The corresponding orbital separation at which the microlensing signal equals the transit signal is 0.046 AU. For an Earth-mass object, the

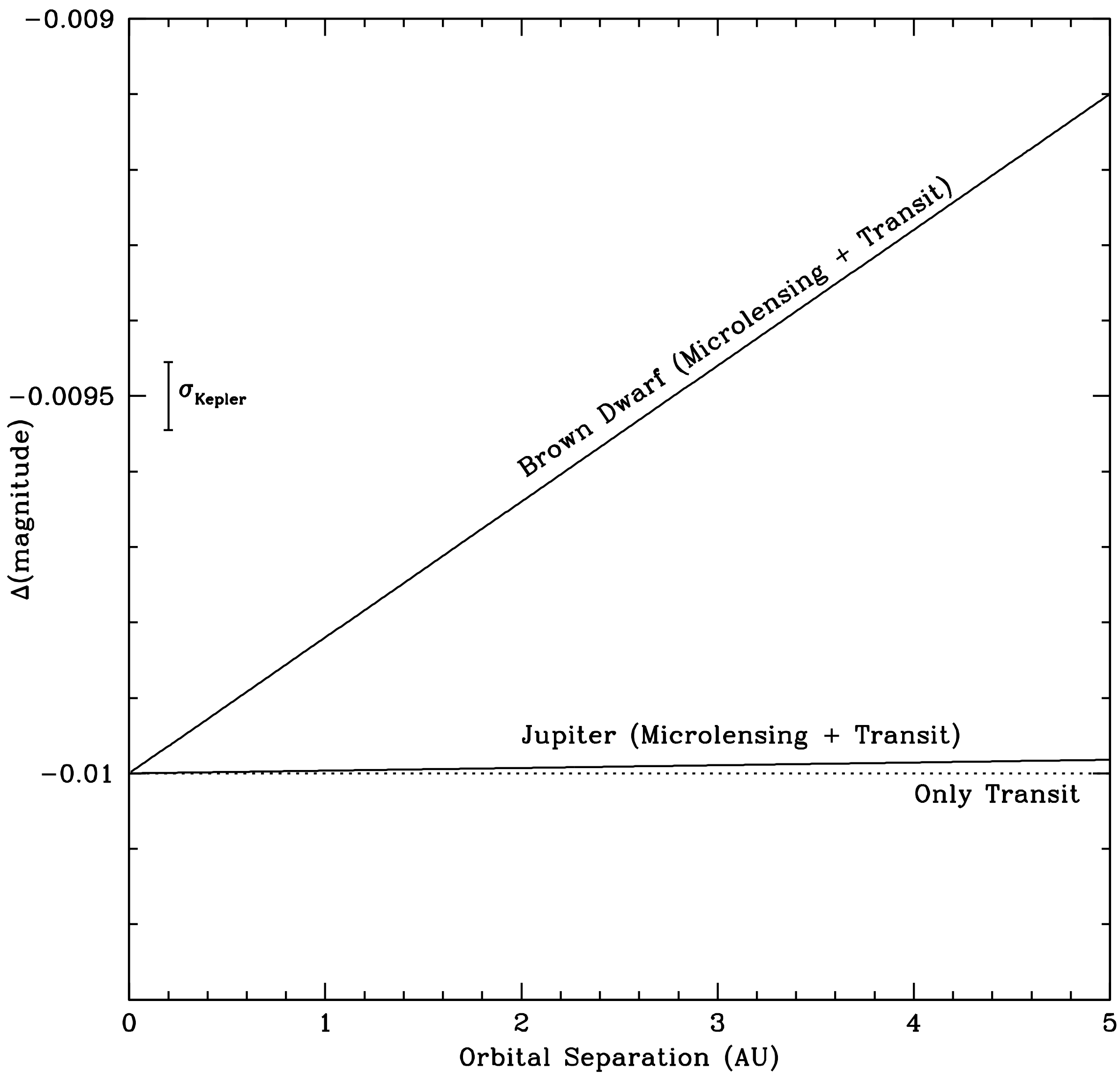

Fig. 6.— Same as the previous figure but the y-scale is enlarged to show in detail the effects of a brown dwarf and a Jupiter-mass planet. At an orbital separation of 1 AU, the the effect of microlensing for a Jupiter-mass planet is negligible. But the effect of microlensing by a brown dwarf is appreciable and must be taken into account in deriving its physical parameters from the photometric observations. At an orbital separation of 5 AU, the effect of microlensing is just noticeable for a Jupiter-mass planet.

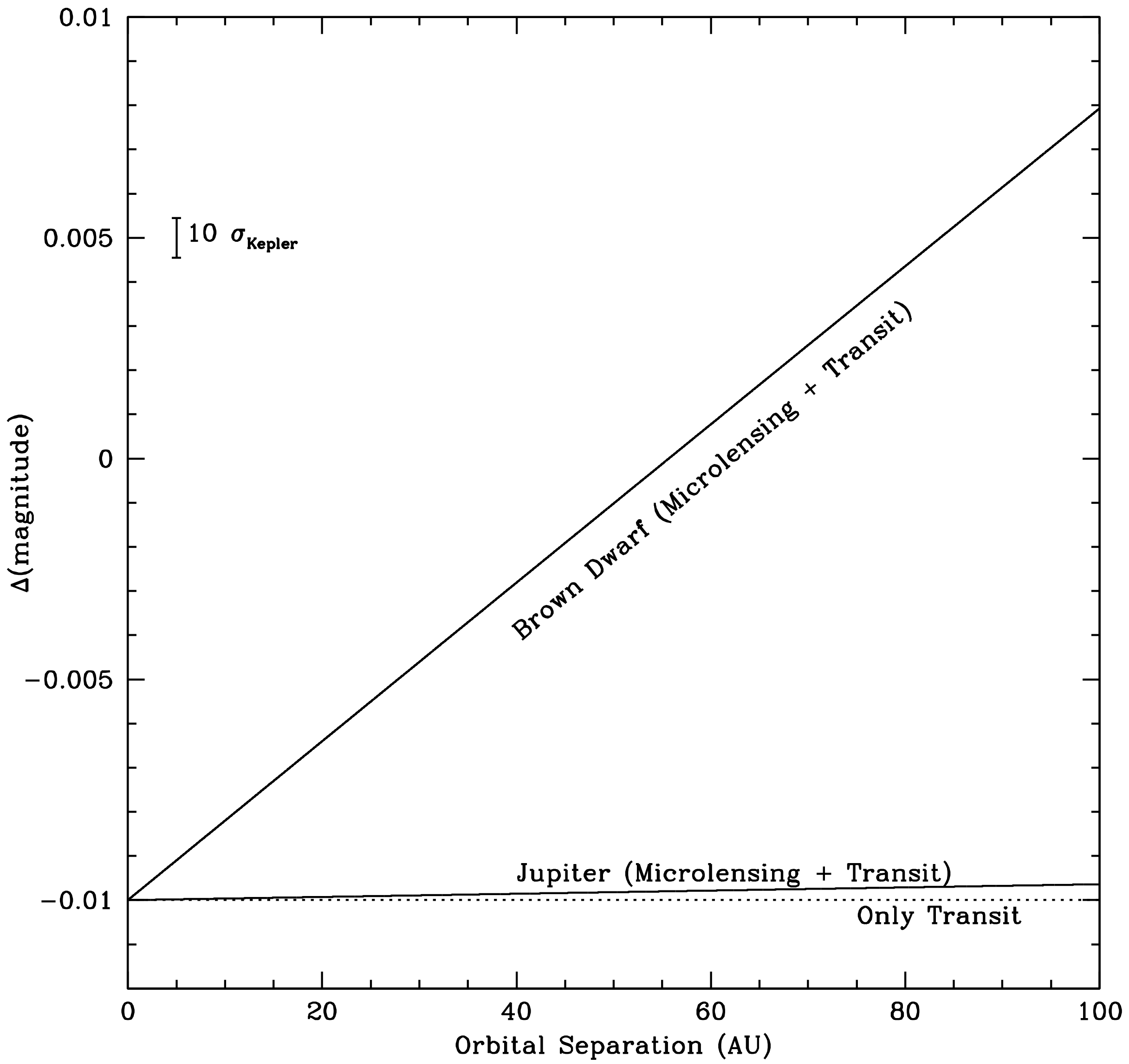

Fig. 7.— Same as the previous figure but for a larger range of orbital separations (0 to 100 AU). This figure shows that for a brown dwarf secondary, the transit signal is fully compensated by the microlensing signal at an orbital separation of ∼55 AU, after which the net effect is a positive amplification.

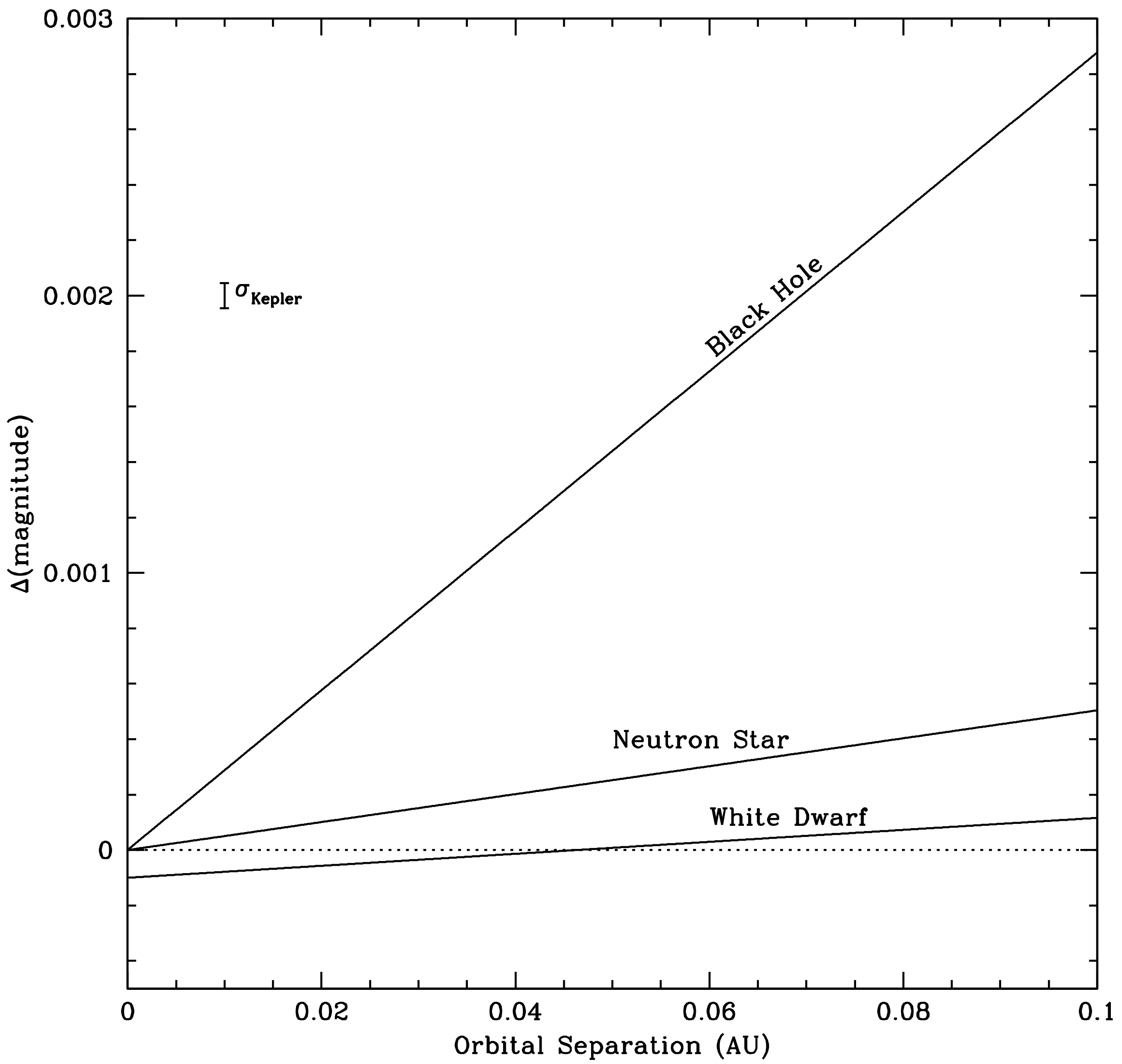

Fig. 8.— The amplifications caused by white dwarf, neutron star and black hole secondaries at small orbital separations (0 to 0.1 AU). In case of the black hole and neutron star secondaries, the microlensing contribution is larger than the transit signal even for the smallest possible orbital radius (when the orbital separation is the same as the stellar radius), so that the net amplification is always positive. For a white dwarf secondary, the net amplification is positive at an orbital separation of 0.046 AU and beyond.

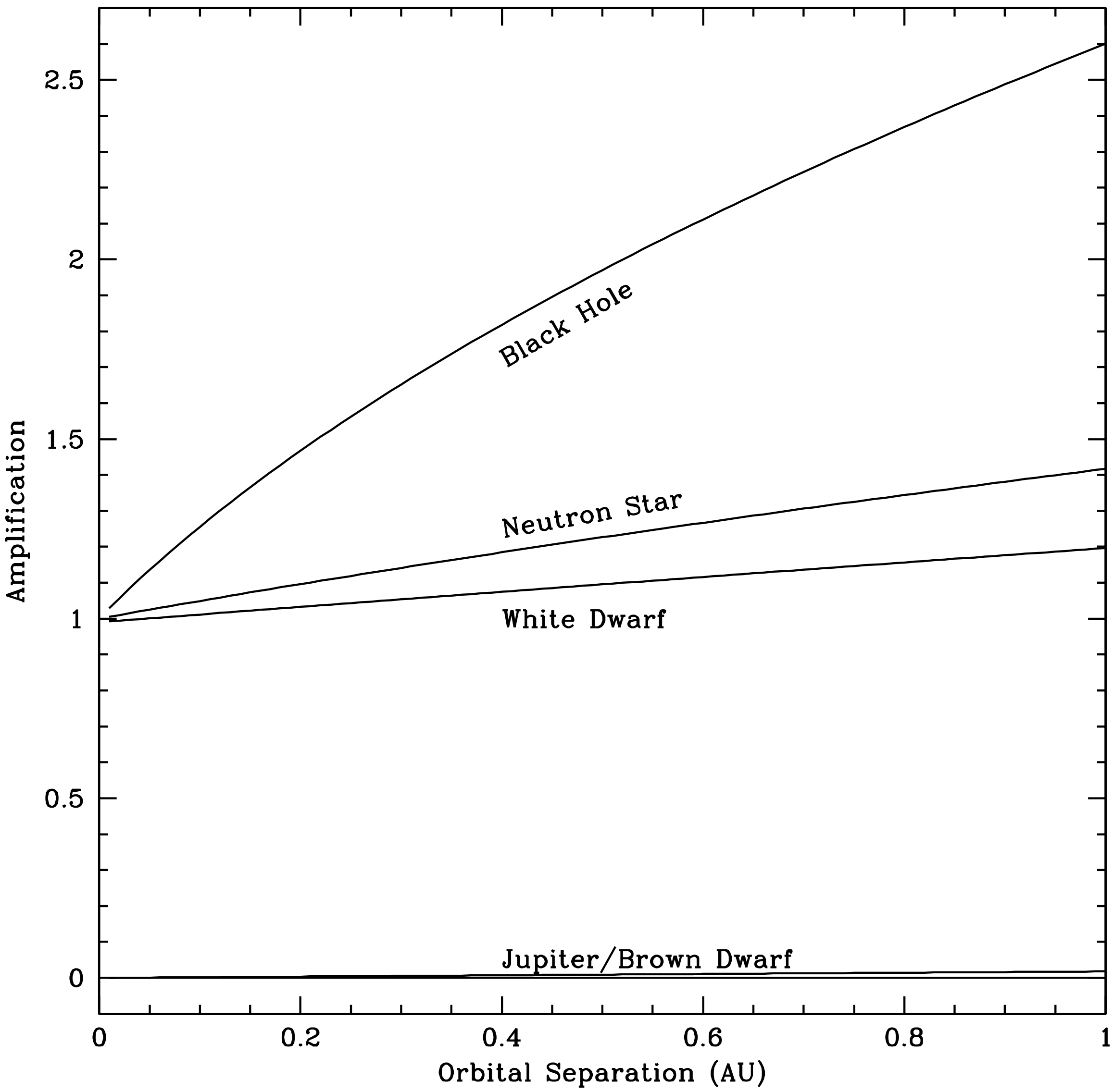

Fig. 9.— The effect of microlensing when the size of the source is 7×10^9 cm, as applicable for a brown dwarf or a Jupiter. The effect is more dramatic when the source size is smaller. The amplification, which is the ratio of the amplified luminosity and the original luminosity, is much larger compared to the earlier case of a solar type source.

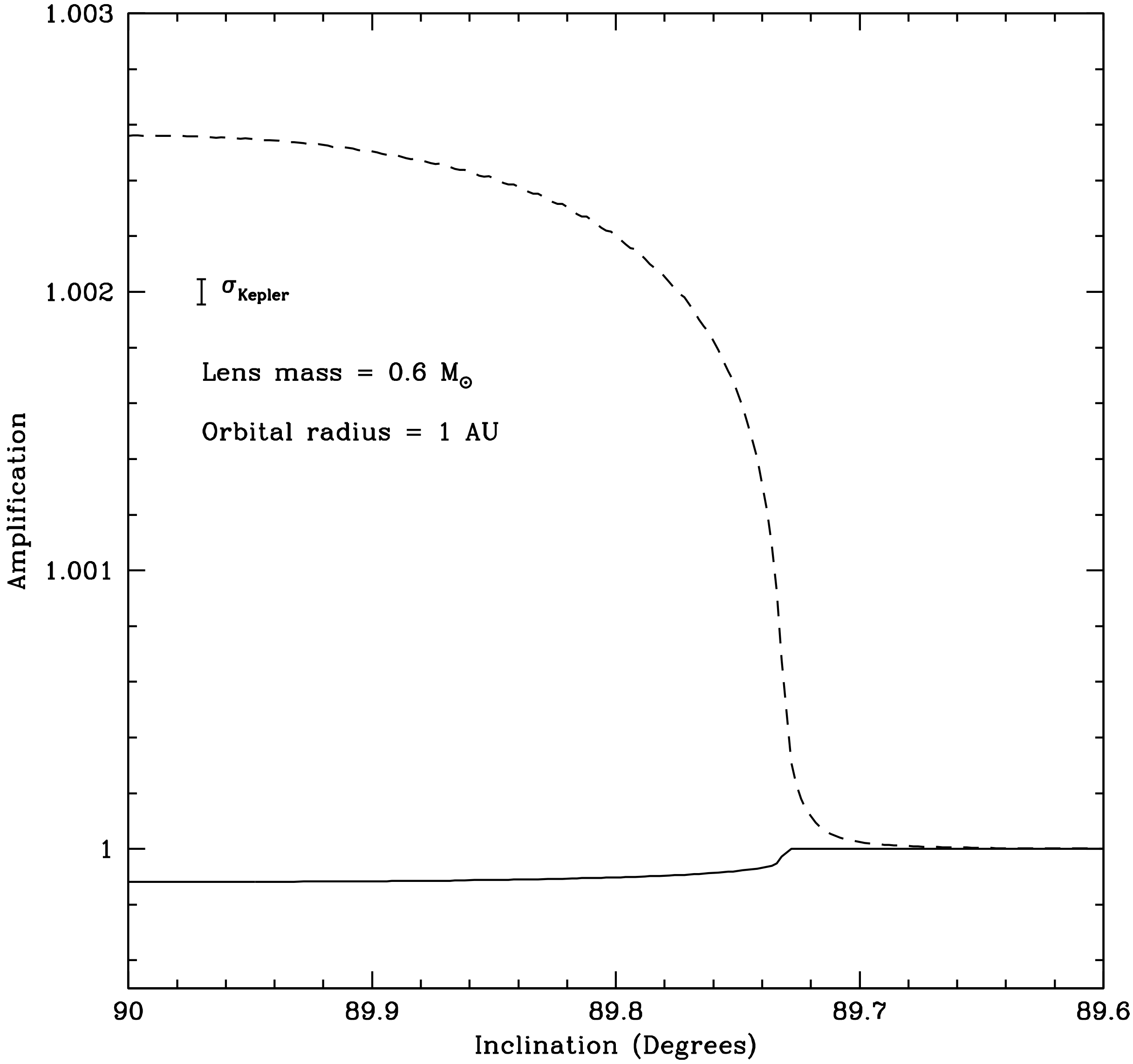

Fig. 10.— The expected maximum amplification caused by a white dwarf at 1 AU from a solar type star is shown here as a function of inclination. The solid curve is the pure transit contribution, and the dashed curve takes both the microlensing and the transit contributions into account. The limb darkening of the source is taken into account in generating the curves.

corresponding orbital radius is ∼2300 AU.

5. Special Cases

5.1. Jupiters and Brown Dwarfs

The radii of brown dwarfs are similar to the radii of Jupiters, so the expected light curves due to their transits would be similar. Thus, a brown dwarf is indistinguishable from a Jupiter from its transit signal alone. However, since the mass of a brown dwarf is considerably larger (15-80 M_{Jup}), the microlensing signal from a brown dwarf would be much larger. For example, Fig. 12 shows the light curves as expected from a Jupiter and a 50 M_{Jup} brown dwarf at 1 AU. The dashed curve shows the pure transit for both objects and the solid curve shows the combined effect of the transit and microlensing for a brown dwarf. For a Jupiter, the combined effect of transit and microlensing is indistinguishable from a pure transit curve. For a brown dwarf, the combined light curve is different from the transit curve. Note that the expected depth in the observed light curve is smaller for a brown dwarf than for a Jupiter, but the shapes of the light curves for both objects are very similar. Thus, there is a degeneracy between the light curves due to a Jupiter and a brown dwarf. It is clear that the contribution due to microlensing must be taken into account in the interpretation of the observed light curves, particularly in estimating the mass/radius of the secondary. Fig. 13 shows the light curves for a brown dwarf at 55 AU which, if observed, would be easy to interpret as due to a brown dwarf since the light curve due to a Jupiter is close to the transit curve itself. Notice that there is a slight positive amplification at the ingress (egress) since the microlensing begins before (ends after) the transit contribution begins (ends). This curve corresponds to an orbital period of 405 yr, and is hence mostly of pedagogical interest since the probability of observing such an event is very small.

5.2. Earths and White Dwarfs

Interestingly, white dwarfs have radii similar to Earth-mass planets. As mentioned earlier, one of the prime objectives of *Kepler* is to detect Earth-mass planets from their transit signals. There has been some concern that the Earth-mass planets would be confused with white dwarfs since their transit signals would be similar. (The secondary eclipse may provide a clear test to distinguish between a white dwarf and an Earth-mass planet, but the secondary eclipse may not be seen in some cases when the orbital eccentricity is high or because the timescale is such that only the primary eclipse is observed). However, as we

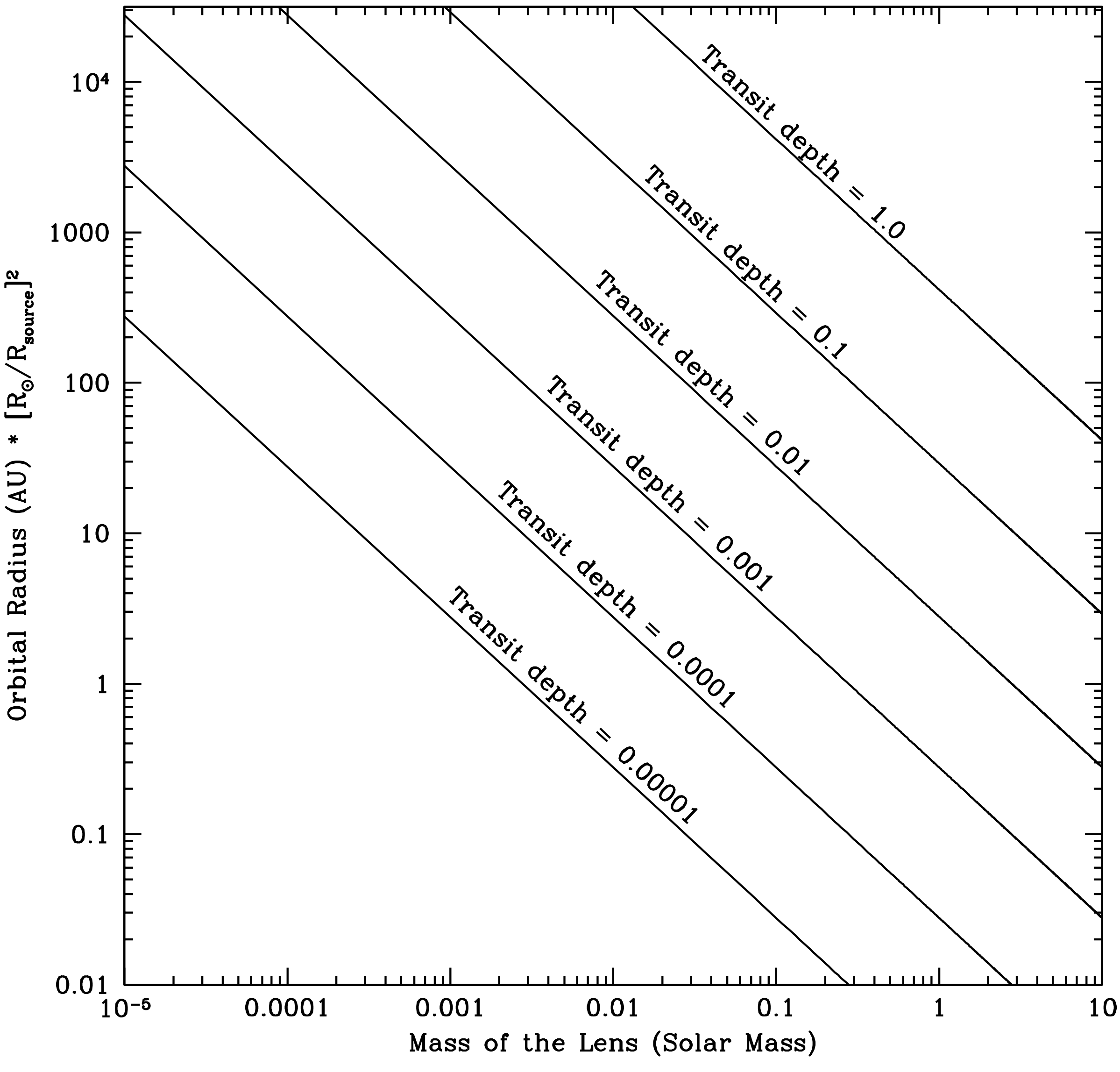

Fig. 11.— The orbital radius at which the microlensing signal is equal to the transit signal is plotted here as a function of the mass of the secondary, for various transit depths. For example, for a white dwarf, the expected transit depth is 0.0001 and the mass of the secondary is $\sim$0.6 $M_{\odot}$. The corresponding orbital radius is 0.05 AU where the transit signal equals the microlensing signal, and beyond which the net amplification is positive.

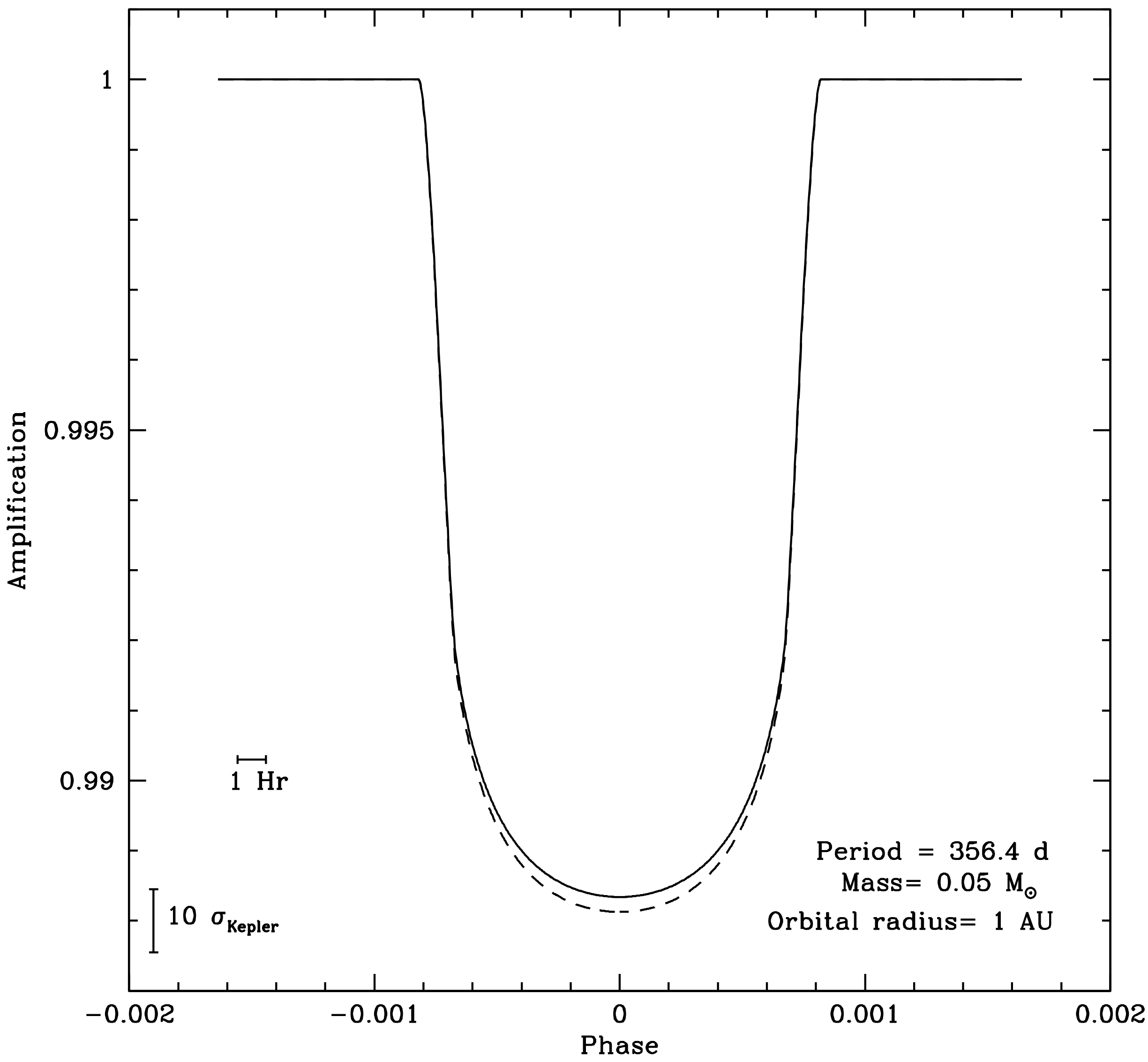

Fig. 12.— The light curves caused by a 0.05 $M_{\odot}$ brown dwarf and a Jupiter at 1 AU from a solar type star. The dashed curve is what one would expect purely from transit. The solid curve shows the combined effect of the transit and microlensing for a brown dwarf. The combined effect of transit and microlensing is indistinguishable from a pure transit curve for Jupiter since the shape of the combined as well as the transit light curves are very similar. The depth of the observed light curve would be smaller for a brown dwarf than for a Jupiter.

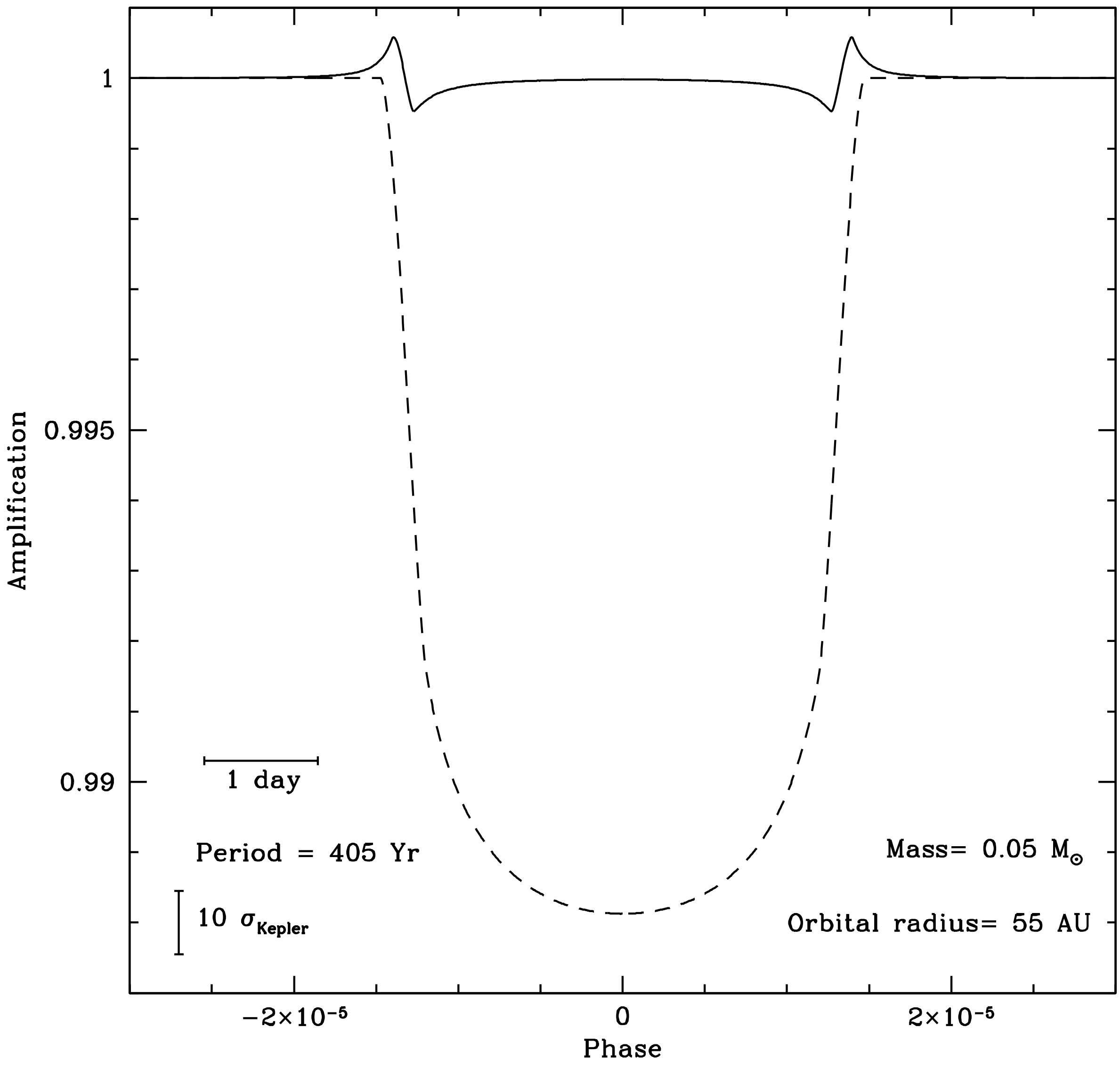

Fig. 13.— The light curves caused by a 0.05 $M_{\odot}$ brown dwarf at 55 AU from a solar type star. The dashed curve is what one would expect purely from transit. The solid curve takes both the transit and the microlensing contributions into account, and hence corresponds to the actual light curve that one would observe. Notice that there is a slight positive amplification at the ingress (and egress) since the microlensing begins before (ends after) the transit contribution begins (ends). This curve corresponds to an orbital period of 405 yr (and is hence mostly of pedagogical interest).

explained in §4, in the case of a white dwarf the effect of microlensing will dominate the signal. Fig. 14 shows the light curves due to a white dwarf secondary at 0.03 AU, 0.0463 AU and 0.1 AU, with corresponding periods of 1.50, 2.88 and 9.13 days, respectively. The dashed curves are the light curves expected from pure transit, and the dotted, solid and dot-dashed curves are the corresponding light curves after taking the microlensing contribution into account. Only at orbital separations smaller than 0.0463 AU would the expected Δmag be negative, with the shape of the observed light curve similar to the transit curves. We note that at an orbital separation of less than 0.01 AU, the primary is likely to fill its Roche lobe (Eggleton, 1983). This will cause mass-transfer from the primary, which may cause light variations much larger than the transit or the microlensing effect. Also, the primary will be tidally distorted producing distinct ellipsoidal variations. Thus, the transit effect may be difficult to observe for separations below 0.05 AU, beyond which the Δmag is expected to be positive.

The expected light curve when the white dwarf is at 1 AU is shown in Fig. 15. In such a case, the white dwarf would be detectable through its positive amplification at >100 σ-level in observations averaged over a single event with *Kepler*!

It is of interest to consider how accurately *Kepler* observations of a White Dwarf transiting a solar-like star in a 1 AU orbit would constrain the lens mass. For such a canonical case (shown in Fig. 15), the maximum amplification is 0.0024 magnitudes. The precision per 15 minute sample for an assumed $V = 12$ star observed with *Kepler* is 90 μmag. Hence, with 40 samples during the 10 hour lensing event, the maximum amplification will be determined to about 15 μmag, resulting in a relative error on A_0 of 0.6%. Given that the mass of the lens scales as the square of the amplification (equations 15-16), and assuming that four events are available for averaging, the relative error contribution for the lens mass from the microlensing observations is also 0.6%. However, equations (15) and (16) also contain the mass and radius of the source star for which we do not have direct values available from the *Kepler* observations alone. Radial velocity observations of even moderate quality would provide a further constraint on the mass, leaving uncertainties on the radius of the source star, r_S, as the likely largest contributing error source. Equation (17) provides a direct constraint on r_S simply from the event width, but the unknown orbital inclination must also be allowed for. Spectroscopic measurements might suffice to constrain r_S at about 10% level, thus the lens mass to 20% level. As was done for HD 209458 (Brown *et al.* 2001), constraints on the source stellar radius may also be derived from the light curve itself, since some subtle details will depend in unique ways on the generally degenerate effect of r_S and M_L in fixing the light curve. Equation (21) provides a further constraint on the lens mass if an estimate of the mass of the primary is available. Note that the orbital inclination and limb darkening parameters can also be estimated from the observed light curve (as was done

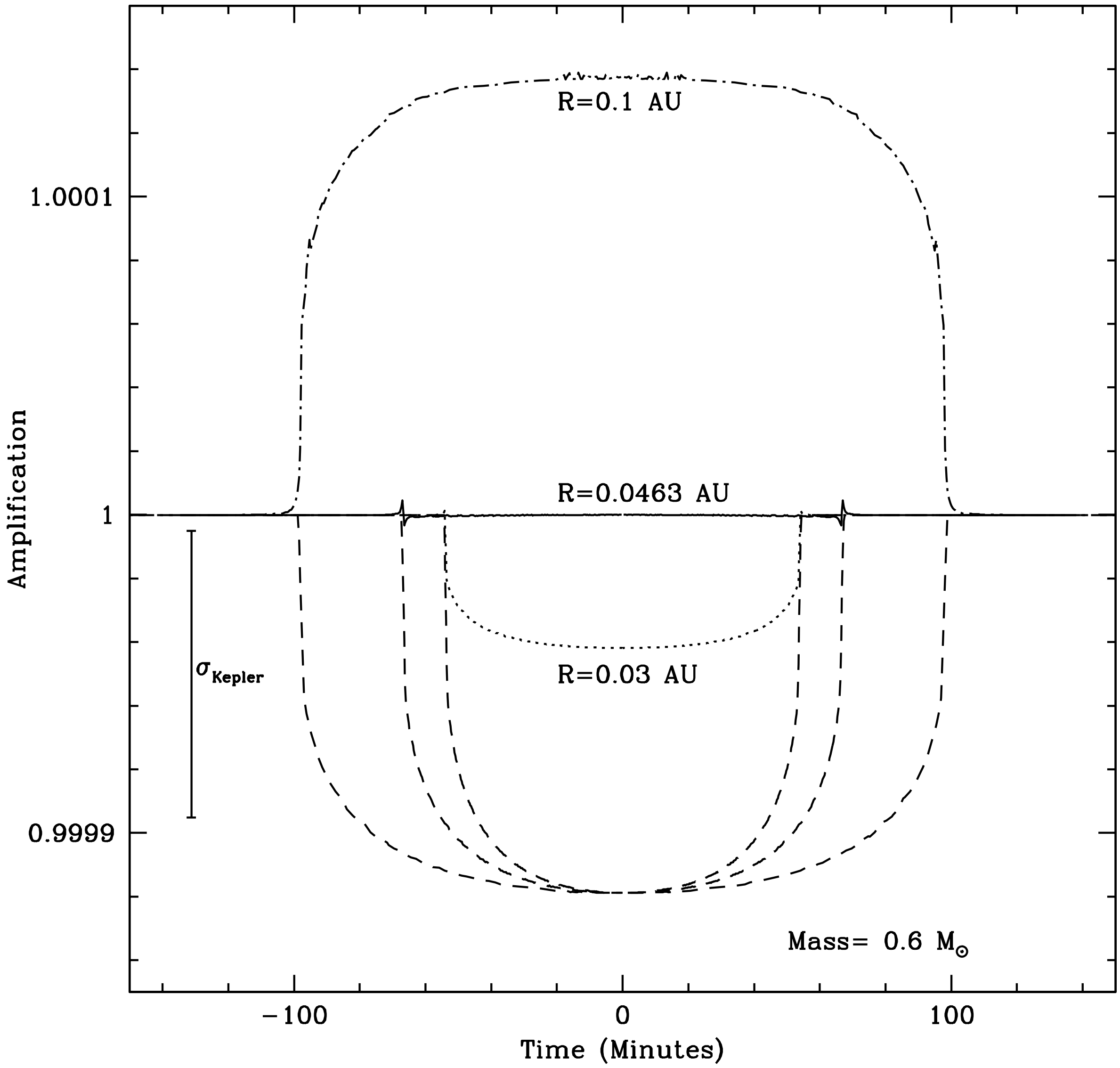

Fig. 14.— The light curve caused by a 0.6 $M_\odot$ white dwarf at 0.03, 0.0463 and 0.1 AU from a solar type star. The dashed curves are what one would expect purely from transit. The corresponding upper curves (dotted, solid and dot-dashed curves, respectively) take both the transit and the microlensing contributions into account, and hence correspond to the actual light curves that one would observe. Notice that, even at a small orbital radius of 0.03 AU (where the white dwarf is likely to produce tidal distortions on the companion), the microlensing contribution is significant. At an orbital radius of 0.0463 AU, the microlensing contribution almost exactly cancels out the transit contribution. At an orbital radius of 0.1 AU, the net effect is a positive amplification which is easily detectable by *Kepler*.

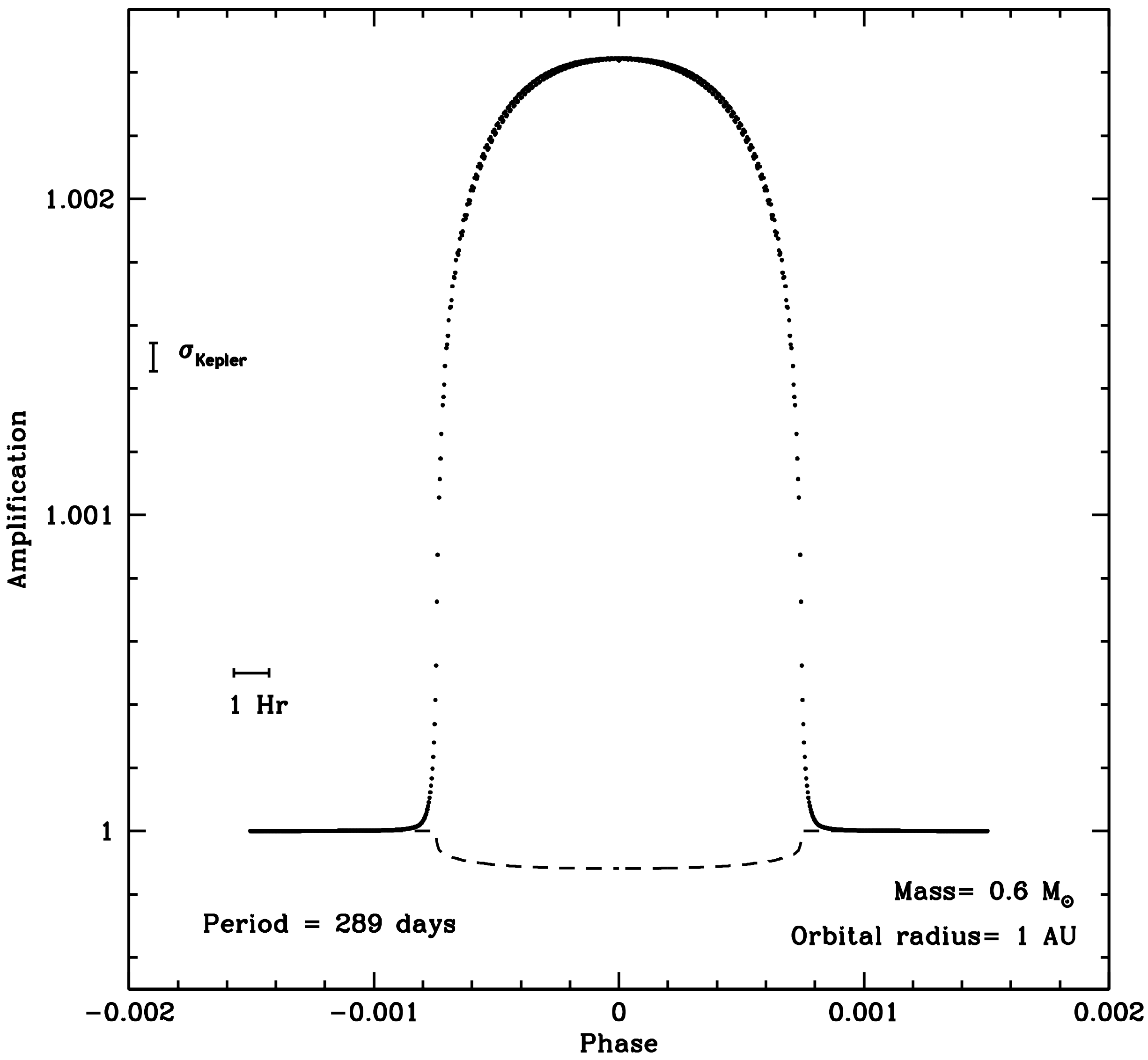

Fig. 15.— The light curve caused by a 0.6 $M_\odot$ white dwarf at 1 AU from a solar type star. The dashed curve is what one would expect purely from transit. The solid curve takes both the transit and the microlensing contributions into account, and hence corresponds to the actual light curve that one would observe. Notice that the white dwarf would be detectable through its positive amplification at > 100 σ-level in observations averaged over a single event with *Kepler*!

for HD 209458), and a detailed treatment of the errors would be required in determining the uncertainties in different physical parameters. Fitting the entire light curve would take all the constraints in a self-consistent manner, providing the best determination of the various parameters, including the lens mass to an estimated accuracy of 1 to 5 percent.

5.3. Neutron Stars and Black Holes

The expected transit signals from a neutron star and a black hole are of the order of nano-magnitudes and smaller. So the transit signal in these cases can be neglected for all practical purposes. In the treatment of microlensing, we note that the deflection corresponding to the fainter image (i.e. the smaller of the two deflections) is larger than the size of the lens even for small orbital separations. So the finite size of the lens can also be ignored. Thus the expected light curve is the same as what is expected from the pure microlensing of an extended source and a point lens, e.g. as in Fig. 15 with amplitude scaled approximately linearly by the lens mass. Note that the expected Δmag from a neutron star and a black hole at an orbital radius of 1 AU are 5 and 28 milli-magnitudes respectively, which may be detectable from ground-based observations.

6. Discussion and Summary

We have shown that near-field microlensing of main sequence stars by orbiting compact companions provides signals that would be easily detected by a space mission such as *Kepler* dedicated to the detection of extrasolar terrestrial planets via transits. For terrestrial planets with orbital periods up to a few years to which *Kepler* has sensitivity to transits, the microlensing contribution to the signal will always be entirely negligible. Jovian class planets in orbits of a few AU provide a microlensing contribution that just starts to be relevant, albeit still small compared to the inherent transit signal. White dwarfs, neutron stars, or black holes transiting a main sequence star in an $\sim$1 AU orbit would provide easily detectable microlensing signatures that swamp any underlying transit signal. Therefore, although the radius of a white dwarf is similar to that of a terrestrial planet, a transiting white dwarf (with an orbital separation of 0.25 - 2.0 AU, which is the region of prime interest for *Kepler*) will not provide a source of false alarms for extrasolar planet detection since the resulting signal will be a significant brightening rather than a small diminution in light.

Compact objects like white dwarfs, neutron stars, and black holes are now easily found when they reside in close orbits ($\lesssim$ 0.1 AU) from a main-sequence companion since they induce ellipsoidal variations in the companion. Furthermore, such systems often become x-ray and radio sources through emissions associated with mass transfer (even when the mass transfer occurs at low levels). While the microlensing signal may be detectable even for an orbital separation as small as $\sim$0.1 AU, other variations (such as ellipsoidal variations caused by the distortion of the companion, variations from star spots for induced rapid rotation) clearly call attention to the presence of a degenerate object in such systems. As an example, we note that KPD 1930+2752 is one such interesting case of a sdB binary in which the unseen companion is likely to be a white dwarf with an orbital period of 0.095 days (Maxted et al. 2000, Billeres et al. 2000).

The microlensing signal for compact objects with orbital separations of $\gtrsim$1 AU will be easily seen by *Kepler*. In such cases, old white dwarfs, neutron stars and black holes would not already have signaled their presence since the wide separation would not induce the canonical signatures discussed above. However, as with extrasolar planet transits, microlensing from orbiting compact objects will only be observed in a very small fraction of cases in which the inclinations happen to be ideal so that transits can be observed. The probability of transits is r_S/a, where r_S is the radius of the primary, and a is the orbital separation. For a solar like star and an object at 1 AU this probability is about 0.005. Thus if all 100,000 stars in the *Kepler* sample have compact objects orbiting within 0.25 to 2.0 AU, some 500 would be detected through their microlensing signatures. If a more physically reasonable fraction of 1% of stars surveyed contain such compact, massive objects then the number detected by *Kepler* would be 5. What, then, are the prospects for observing compact objects via microlensing signatures by *Kepler*? Duquennoy & Mayor (1991) and Heacox & Gathright (1994) show that about two-thirds of G-type stars are binaries, and that about 20% of them have periods between 0.25 and 2.0 years. Thus, for the *Kepler* mission to detect a statistically modest total of 5 systems with microlensing in such circumstances, $\sim$7.5% of binary systems must contain a compact object (most likely a white dwarf). By comparison, the observed white dwarf fraction in the solar-age open cluster M67 is about 9% by mass (Richer et al. 1998), and since incompleteness may still be important in this case, this is a lower limit to the detected cluster white dwarfs. This suggests that the overall fraction of white dwarfs is sufficient to yield several detections during the *Kepler* mission. Estimates of the fraction of baryonic mass in compact objects in the local disk typically span values of 10 – 30% (e.g. Weidemann, 1990). This, in turn, implies that the detected number of such microlensing systems will be able to place interesting constraints on the fraction of stars having compact companions.

For microlensing detections from systems where the orbital period is known from repeated events, it will be possible to determine the mass of the compact object directly from the amplitude of the microlensing signal (assuming independent information on the primary main sequence star is available). For the case of white dwarfs, information on the compact object may also be available if the secondary eclipse is observed, and radial velocity followup observations will be able to determine independent mass estimates.

We thank Meena Sahu and Mario Livio for useful discussions. We wish to thank the referee, Scott Gaudi, for useful suggestions.

REFERENCES

Afonso, C., et al. 2000, ApJ, 532, 340

Agol, E. 2002, ApJ, in press (astro-ph/0207228)

Albrow, M. et al. 2001a, ApJ, 556, L113

Albrow, M. et al. 2001b, ApJ, 549, 759

Alcock, C. et al. 2000, ApJ, 542, 281

An, J.H. et al. 2002, ApJ, 572, 521

Beskin, G.M., & Tuntsov, A.V. 2002, A& A, in press (astro-ph/0208095)

Billeres, M., Fontaine, G., & Brassard, P. 2000, ApJ, 530, 441

Bontz, R.J. 1979, ApJ, 233, 402

Borucki, W.J., & Summers, A.L. 1984, Icarus, 58, 121

Bromley, B. C. 1996, ApJ, 467, 537

Brown, T. M., Charbonneau, D., Gilliland, Ronald L. D., Noyes, R. W., & Burrows, A. 2001, ApJ, 552, 699

Claret, A., & Gimenez, A. 1990, A& A, 230, 412

Dominik, M., & Hirshfeld, A. C. 1996, A& A, 313, 841

Dominik, M. 1998, A& A, 333,79

Duquennoy, A., & Mayor, M. 1991, A& A, 248, 485

Eggleton, P.P. 1983, ApJ, 268, 368

Gaudi, B.S. et al. 2002, ApJ, 566, 463

Gould, A. 1995, ApJ, 446, 541

Gould, A., & Gaucherel, C. 1997, ApJ, 477, 580

Gould, A. 2001, PASP, 113, 903

Heacox, W.D., & Gathright, J. 1994, AJ, 108, 1101

Lasserre, T. et al. (EROS Collaboration), 2001, A& A, 355, L39

Marsh, T. R. 2001, MNRAS, 324, 547

Maxted, P.F.L., Marsh, T.R., & North, R.C. 2000, MNRAS, 317, L41

Paczyński, B. 1996, Ann. Rev. Astron. Astrophys. 34, 419

Richer, H.B., Fahlman, G.G., Rosvick, J., & Ibata, R. 1998, ApJ, 116, L91

Sahu, K.C. 1994a, Nature, 370, 275

Sahu, K.C. 1994b, PASP, 106, 942

Schneider, P., & Weiss, A. 1992, A& A, 260, 1

Schneider, P., Ehlers,J., & Falco, E.E. "Gravitational Lenses", Springer-Verlag, 1993

Udalski, A. et al. 2000, Acta Astron., 50, 279

Weidemann, V. 1990, in *Baryonic Dark Matter*, D. Lynden-Bell and G. Gilmore (eds.), Kluwer Publishers, p. 87.

Witt, H.J. & Mao, S. 1994, ApJ, 430, 505